Characterization of the interfacial shear strength of glass-fiber reinforced polymers made from novel RTM processes

B. Haspel, C. Hoffmann, P. Elsner, Kay A. Weidenmann

Angaben zur Veröffentlichung / Publication details:

Haspel, B., C. Hoffmann, P. Elsner, and Kay A. Weidenmann. 2015. "Characterization of the interfacial shear strength of glass-fiber reinforced polymers made from novel RTM processes." *International Journal of Plastics Technology* 19 (2): 333–46. https://doi.org/10.1007/s12588-015-9122-3.

Characterization of the interfacial shear strength of glass-fiber reinforced polymers made from novel RTM processes

B. Haspel[1] · **C. Hoffmann**[1] · **P. Elsner**[1] · **K. A. Weidenmann**[1]

Abstract In this study, three different glass fiber reinforced polymers have been investigated with respect to the interfacial shear strength. Conventional resin transfer molding (RTM) and the compression RTM (CRTM) process for the production of reinforced samples with an epoxy matrix were chosen. The third process was a thermoplastic RTM (TRTM) process for producing composites with a thermoplastic polyamide 6 matrix. Fiber type and coupling agent were not varied. The interfacial shear strengths reached by the different processing routes were determined by push-out tests. It is shown that the RTM interface shear strength is very high and comparable to that generated by the CRTM process, despite increased fiber fracture for the RTM samples. The TRTM process yielded significantly lower interfacial shear strength values. Plastographic analysis of the material systems showed the formation of an interfacial layer between the fibers and the thermoset matrix. For the thermoplastic matrix a significant lower formation of crystalline spherulites at the interface and no interfacial layer could be observed.

Keywords RTM · Composites · Push-out test · Interfacial layer · Debonding · Coupling agent

Introduction

The mechanical properties of fiber reinforced plastics are highly dependent on the properties of the fiber-matrix interface [1–3]. These includes a continuous contact

✉ K. A. Weidenmann
kay.weidenmann@kit.edu

[1] Institute for Applied Materials (IAM–WK), Karlsruhe Institute of Technology (KIT), Engelbert-Arnold-Strasse 4, 76128 Karlsruhe, Germany

between the two components to ensure a homogeneous load transmission and fewer stress peaks, as well as good adhesion between fiber and matrix [4]. As the adhesion is influenced by processing routes and parameters, a thorough characterization of the interfacial shear strength is necessary for further process development or optimization. This includes the characterization of novel processing routes as it is done in this contribution.

A basic view of the nature of the interface of composite materials is carried out by K. L. Mittal [5]. According to this theory, there are various explanations for the adhesion between the two components. In detail the chemical and mechanical influences are referred to be the main contributors of adhesive strength between fibers and matrix. Other effects like adhesions due to friction, electrostatic effects, interdiffusion of long chain molecules in polymers and the physical stabilization by energy release in the creation of more favorable interfaces, are to be regarded as negligible [4, 6]. However, there is no chemical bond directly between fiber and matrix. This chemical bond is supported by an applied interlayer due to coupling agents [7]. These coupling agents are bonded to the fiber surface and form a three-dimensional siloxane network which covers the fiber surface [7–9]. The connection to the surrounding polymer matrix, occur either by a direct reaction with the resin [6] or through an interdiffusion [8], especially in thermoplastic matrix materials [10]. Whether a geometric boundary layer occurs remains questionable and also the effect on the mechanical properties of the matrix show inconsistencies in the literature [11, 12]. However, the positive effect of increasing the interfacial strength is well known and widely used in industry [13–15]. Also, the morphology of the matrix is, especially in the interfacial area, very important [16]. According to the anisotropic properties of the spherulites, which are formed due to a directional polymerization, the interfacial strength can be enhanced [17].

To determine the interfacial shear strength between fiber and matrix, there are a number of tests which differ in set-up, procedure and interpretation of results, such as the microbond test [18], the push-in test [19], the fragmentation test [20] or the pull-out test [21–23]. However, one of the most important methods used is the push-out test presented by Marshall in 1984 [24].

For this test thin samples with vertically oriented fibers are required to enable complete separation of the fibers under stress. These samples are clamped on a perforated plate, through which the fibers are pushed using a flat-punch indenter. The interfacial properties can be characterized by the average interfacial shear strength with respect to the outer surface of the embedded fiber and by observation of the maximum load [25, 26]. More complex calculation models, which predict a failure of the interface, based on the shear lag models, originally presented by Cox [27], were continuously improved [28–33]. However, an exact calculation is still difficult due to the assumption of exponential shear stress distributions [34].

In general, the interfacial failure, caused by the push-out tests, is characterized by stable crack propagation. Whether this delamination starts from the top or from the bottom of the specimen depends on the ratio of the stiffness of the matrix fiber [35], as well as the ratio of fiber radius to the radius of the perforated plate [36].

Even if the various testing methods predict due to the different geometries partially different interfacial shear strength for the same fiber/matrix systems [37–40], under the same test conditions comparison measurements between the various composite materials can be made. Thus, the push-out method was chosen for this work.

Experimental

For the investigated composite materials the same reinforcing fibers were used for all processes. The fiber layers were a quasi-unidirectional fiber fabric of the company Interglas at which 90 % of the fibers were oriented in one direction, and the remaining 10 % were cross-woven to it. According to the manufacturer the used coupling agent FK800 is suitable for thermoset as well as thermoplastic matrix systems. The used matrix systems were selected according to the different RTM processes.

As a reference, a conventional RTM process with increased injection pressure of 20 bar was chosen [41]. As second process a Compression RTM route was used. The process is very similar to the conventional RTM process, with the difference that the mold is not fully closed after insertion of the preform. Instead, the resin-hardener mixture is injected, which is distributed to and partly in the preform. Afterwards the mold will completely closed [42] and the fabric completely infiltrated by the resin. The injection into the cavity has a substantially lower resistance compared to the conventional RTM process, whereby the injection time is reduced to a minimum [43]. For both processes the thermosetting epoxy resin XB3585 XB3458 from Huntsman International LLC was used as matrix system. As the third process the Thermoplastic RTM process was chosen. The thermoplastic RTM (TRTM) is a technology recently developed at the Fraunhofer ICT (Pfinztal, Germany) [44]. This novel adaptation of the RTM process for thermoplastics is essentially based on the structural reaction injection molding (SRIM) process [45]. At the TRTM process a monomer melt of low viscosity with an additional catalyst and an activator will be injected under high pressure into the mold, where it then polymerized to polyamide 6 [46]. All three RTM processes are available at the Fraunhofer ICT in Pfinztal where the test sheets were produced.

For the push-out tests themselves thin sections were prepared from the manufactured sheets. It was taken care that the samples were cut out perpendicularly to the main direction of the fibers. Thus 90 % of all fibers were oriented orthogonally to the base level and therefore theoretically suitable for push-out tests. Therefore, a single sample has enough fiber for indentation. To handle the deviation of the results due to the sample preparation three samples of each process with good surface quality were selected.

The experimental set-up was constructed according to the schematic diagram of [2], wherein the push-out samples were clamped on a perforated plate which was illuminated from below in order to identify the sites at which the fiber could be pushed out of the matrix. The indentation itself was performed on a Zwick ZHU 0.2 microhardness tester. For the indenter a flat-punch nanoindenter from MTS Nano Instruments (USA) was used which was adapted to the Zwick test rig. This indenter was already used by [47] for push-out tests on alumina wire reinforced aluminum.

Via the live image with 1200× magnification suitable fibers for push-out were selected and the corresponding diameter d_{Fiber} was determined. It was ensured that the fibers were above a hole in the perforated plate and that no fiber-fiber contact was present. After choosing a suitable fiber, the load unit was positioned over the fiber and the indenter was attached step by step by probing with a tactile measuring foot. The actual load during the push-out experiment was carried out position controlled with a loading rate of 0.003 mm/min. Also during the experiment, the load-displacement

curve was recorded. The test was stopped manually, depending on the different detected damage evaluations. In Fig. 1 the optical micrographs a sample before and after the push-out test is shown.

Results

The first evaluation was to characterize the recorded load-displacement curves in five different types which are shown in Fig. 2. This was made to get a better overview about the damage evaluation of the different samples. It shall be noted that it is not possible make any predictions about the actual interfacial shear strength from the load-displacement curves in Fig. 2 because of the missing fiber diameter and the thickness of the tested sample.

Curve type 1 shows an assumed to be ideal push-out curve [33]. By setting losses in the clamping the load increases linearly up to 0025 N. This is followed by the actual elastic deformation of the sample, which is recognized by a steeper linear increase of the load. After this linear load increase a non-linear region occurs, caused by local debonding [2]. According to [35] the seamless transition between the elastic region and local debonding is an indicator of a crack initiation at the lower end of the fiber, which is also due to the large ratio of the elastic moduli of fiber and matrix ($E_{Fiber}/E_{Matrix} \approx 20$). The small ratio of specimen thickness and hole diameter of the perforated plate also promote a crack initiation from below [48]. The debonding continues with stable crack growth along the interface towards the upper end of the fiber [32]. When the critical crack length is reached, the load exceeds the shear strength, which results in an unstable crack growth up to the complete debonding of the fiber [35]. This causes a drastic load drop which can be clearly seen at the curve type 1. The subsequent frictional slip process is demonstrated by a linear decrease of the load, because the contact area between fiber and matrix is getting smaller by continuing the experiment [49]. Considering the tested fiber before and after the push-out test, the fiber appears much darker than before testing. According to [50] this is a clear indication of a broken fiber, which must therefore have occurred during the push-out test. According to Bechel and Sottos [35], the nonlinear load increase could be influenced not only the local debonding also by the fiber breaks. Because of the higher loads and therefore higher

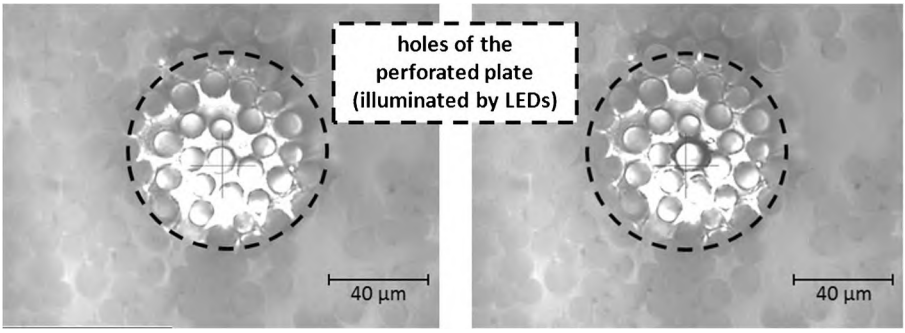

Fig. 1 Optical micrographs of the CRTM sample before (*left*) and after (*right*) the push-out test

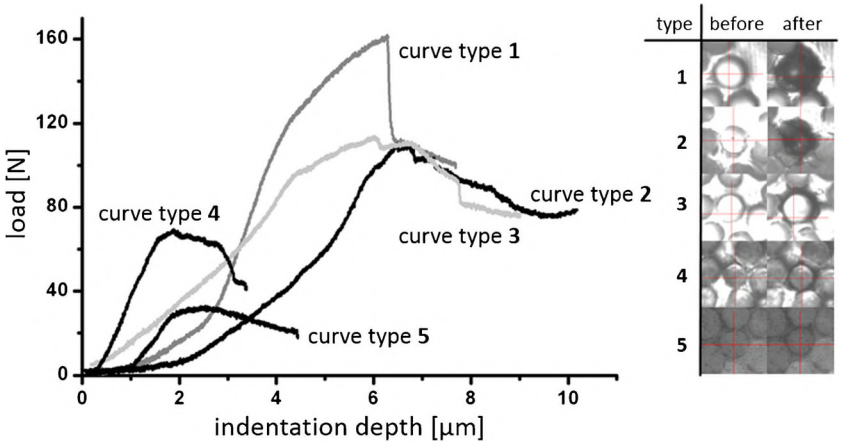

Fig. 2 Different load-displacement curves (*left*) and optical micrographs of the samples before and after the push-out test (*right*)

contact forces between the indenter and the matrix, broken fibers were often detected at thicker samples. However, a clear fiber push out on the downside of the sample was detected, why the test is valid.

Curve type 2 of the load-displacement curves displays a direct transition to slipping at the interface upon reaching the maximum load. This indicates a stabile crack propagation till the complete debonding. On this curve types a fiber break in the contact area of the indenter was also recognized.

That the reason of fiber breaks is not only because of high loads in the contact area of the indenter is shown in curve type 3. The maximum load is comparable to curve type 2, but no fiber break could be detected. However, at a load of approximately 100 mN the load-displacement curve is no longer elastic and the slope is reduced. Unlike for glassfiber reinforced polymers the debonding starts in curve type 3 most probably from the top side of the sample [35]. Thus the tension maxima on the upper crack tip is not on the sample surface where the indenter additionally axially loaded the sample. Therefore the overall load is lower at the upper sample surface [51, 52].

Load-displacement curves of type 4 are very similar to type 1 curves till the point of the maximum load. After reaching the maximum load, the load is nearly constant. During this approximately 1 to 2 µm displacement stabile crack propagation is expected. After that plateau the normal debonding can be seen. This curve types occurred at thinner samples why the maximum load was also notable reduced and no fiber breaks could be determined.

For extremely thin samples curve type 5 could be observed. The maximum load is low and a permanent stabile crack propagation is recognizable. Unlike the curve type 4, the load-displacement curves type 5 shows no plateau at the maximum load and the crack at the interface is stabile till the end. Fiber breaks could not be observed.

Experiments where no reduction of the load in the load-displacement curves and/or push out of the fiber on the bottom of the sample could determined, were declared invalid. The percentage of the different curve types 1–5 is shown in Table 1 for the different processes.

Table 1 Percentage of the different curve types

Curve type	1	2	3	4	5
RTM	19 %	26 %	28 %	19 %	9 %
CRTM	8 %	18 %	38 %	30 %	8 %
TRTM	3 %	14 %	6 %	22 %	56 %

The interfacial shear strength τ was determined by using the following formula (1) [24]. Therefor the previously determined sample thickness t, the fiber diameter d_{Fiber} and the maximum load $F_{\max}$ from the recorded load-displacement curve were used.

$$\tau = \frac{F_{max}}{\pi \, d_{\mathrm{Fiber}} \, t} \tag{1}$$

The obtained mean interfacial shear strength of the different RTM processes are summarized from Tables 2, 3 and 4.

To reduce effects to the interlaminar shear strength due to the sample geometry or the preparation three sample of each process were tested. From the sample specific mean value a total value for every process was calculated, which represents the interlaminar shear strength of the different processes in later discussions.

The experimental results itself shows a relatively high scatter of the standard deviation for all processes. Occasionally this scattering is attributed to different failure mechanisms, which could be observed during the testing of the different processes. These failure mechanism were also shown in the load-displacement curves and correlated as described before.

Discussion

In a direct comparison of the two thermoset RTM processes (RTM and CRTM) the measured interfacial shear strengths are similar. Obviously this is caused by the same material system. In microscopic investigations no major differences in infiltration and fiber distribution can be seen, which was also confirmed by measurements of the porosity and the fiber content. A comparison of the measured interfacial shear strengths with values from the literature confirms the high values [15, 53]. Also the load-displacement curves are tendentially equal. It can be seen that the curve types 2, 3

Table 2 Interlaminar shear strength of the conventional RTM-samples

Process RTM	Number of tests	Thickness t [µm]	Interlaminar shear strength τ [MPa]
Sample 1	23	58	78,2 ± 12,6
Sample 2	10	44	73,5 ± 8,6
Sample 3	10	50	84,7 ± 9,1
Total	43	-	78,8

Table 3 Interlaminar shear strength of the CRTM-samples

Process CRTM	Number of tests	Thickness t [μm]	Interlaminar shear strength τ [MPa]
Sample 1	20	51	80,5 ± 11,7
Sample 2	10	60	72,1 ± 5,4
Sample 3	10	46,5	81,3 ± 7,6
Total	40	-	77,9

and 4 are characteristic for the thermoset RTM processes. Only the high amount of the type 1 load-displacement curves at the conventional RTM process is different from the CRTM process. This can be explained by the later discussed fiber breaks.

The generally very high interfacial shear strength between the glass fibers and thermosetting epoxy resin raises further questions. Due to the general gradation of the strength of polymers the measurable interfacial shear strength should always be less or equal than the matrix shear strength [54].

$$\begin{array}{ccccccc} \text{shear strength} & < & \text{tensile strength} & < & \text{compressive strength} & < & \text{flexural strength} \\ \tau_m & < & R_m & < & R_d & < & R_b \end{array}$$

Since for the tensile strength of the pure epoxy matrix $R_{m,EP}$ a mean value of 69 MPa was determined, normally the measured interfacial shear strength should not exceed this value. The fact of measured interfacial shear strength of about 80 MPa admits two assumptions. Firstly, that a strong bond at the interface exists, on the other hand, it also indicates the formation of an interfacial layer between the fiber and matrix, as has been frequently observed [11, 14, 55]. It is assumed that the interfacial layer covers the fiber completely and having higher strength than the pure epoxy resin, as shown in Fig. 3.

Thus, the measured interfacial shear strength would increase. When considering the shear strength according to Eq. (1) the assumption can be made that the failure at the interface B takes place by the following condition:

$$R_{m,EP}\, r_0 \geq \tau\, r_i \tag{2}$$

Using the measured average values $R_{m,EP}, \tau$ and the also measured average fiber radius of r_i = 4.7 μm, results in a mean radius of the outer interfacial layer of approximately $r_0 \geq$ 5.4 μm. Thus, at least a 0.7 μm thick interfacial layer with increased

Table 4 Interlaminar shear strength of the TRTM-samples

Process TRTM	Number of tests	Thickness t [μm]	Interlaminar shear strength τ [MPa]
Sample 1	16	90	20,4 ± 10,3
Sample 2	10	41,5	33,6 ± 8,3
Sample 3	10	47,5	27,6 ± 6,5
Total	36	-	27,2

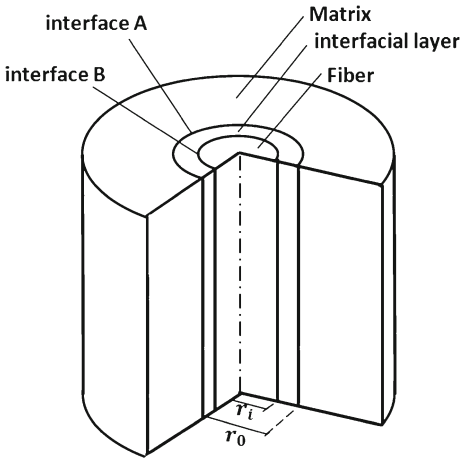

Fig. 3 Scheme of an embedded fiber with interfacial layer: fiber radius -r_i, Outer radius interfacial layer - r_0

mechanical characteristics ($\tau_{m,EP}$> 80 MPa) should be developed to obtain failure at the interface B. To prove that theory SEM images of the tested fibers were observed, as seen in Fig. 4.

The SEM micrographs reveal no clear interfacial layer at the extruded fiber ends. Also an attempt by inking the remained matrix material gave no further information. However, the finite element calculation by Kim et al. [21] showed a maximum stress between fiber and interfacial layer, which promotes the theory of failure at the interface B. Due to the high fiber volume content, many fiber-fiber contacts are visible. In these areas the interfacial layers will overlap and thereby the chemical bonds at the coupling agent can spread from fiber to fiber. This would encourage further strengthening of the matrix properties. Thus, the strength of the interfacial layer seems to rise so far that the shear strength exceeds the interfacial shear strength between fiber and matrix. That would support a failure at interface B.

Additionally to the measured interlaminar shear strength values the occurrence of the fiber breaks during the push out tests were observed. Like already explained the fiber breakage was determined with a transmitted light microscopy [50]. Also, the load-displacement curve type 1 can also caused by fiber breaks during the push out test [35]. The fiber failure itself, as shown in Fig. 5, is caused by local stress concentrations.

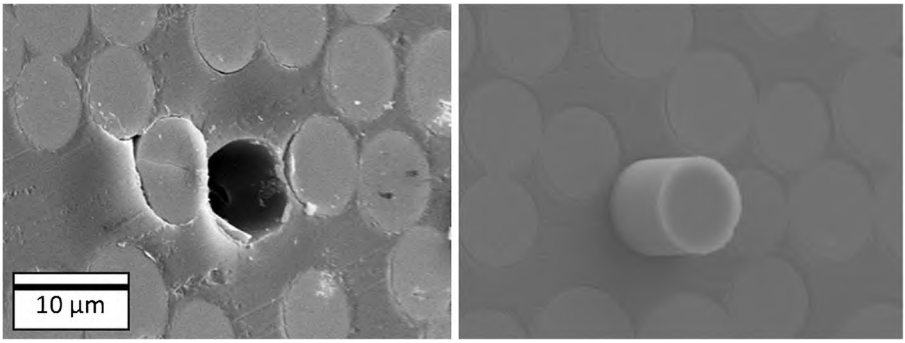

Fig. 4 SEM images of a push-out indentation (*left*) and a push-out extrusion (*right*)

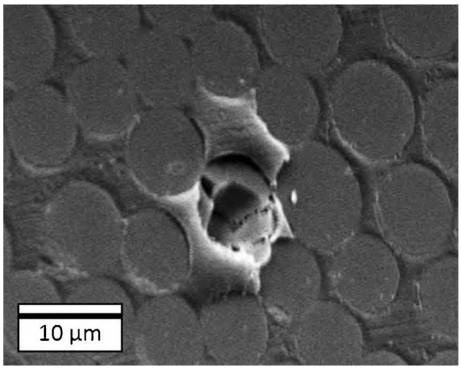

Fig. 5 Fracture surface of a tested fiber

Minimal irregularities on the surface of the sample or the indenter may mar an even placement which results in a high contact stress that occurs at the edge of the indenter.

Although the detected modes of failure are most common at "sharp" indenters such as a Vickers indenter, such a failure mode is also possible with a flat punch indenter and a sufficient overload, according to [56]. In general, in this work the fracture of the fibers could not be associated with a decrease in the interfacial shear strength. Also that the fiber breakage initiates debonding cannot be confirmed, since the debonding most likely begins at the bottom of the fiber [35, 48].

A comparison of the transmitted light microscopies showed a strong dependence between fiber failures and the different sample geometries. The surface analysis of the tested fibers showed that above 80 % of the fibers were broken during the push-out test of conventional RTM sample. At the push-out tests of a CRTM sample with comparable thickness, interlaminare shear strength and consequently equal maximal load, the rate of damaged fibers in the contact area of the indenter was just about 15 %. This Effect can be explained with a top debonding at the CRTM sample, justified by a high amount of load-displacement curves type 3 at the CRTM sample and type 1 at the conventional RTM sample. The difference can be explained as follows.

In addition to the predicted stress concentration at the bottom of the push-out test is still a further maximum at the upper end of the fiber. There is a maximum shear stress through the material resistance and a maximum axial stress due to the indentation and residual stresses. In addition, there are also radial stresses due to residual stresses [51, 52]. Since the global maxima of the shear and radial stress always concentrate at the crack tip, a stable top debonding would effect a shift of the stress maxima, whereby the complex stress state is abrogated at the upper end of the fiber. According to [35] a top debonding will cause a reduction of the measured load at the transition from elastic deformation to the debonding or at least a significantly decline of the slope in the load-displacement diagram. This effect can also be seen at the less damaged sample of the CRTM process in Fig. 6.

Irregularities during the preparation of the thin samples can be mentioned of a reasons for the possible top debonding at the CRTM sample. Damage to the interface at the upper surface by the grinding process would promote a local cracking. It is also feasible that in the CRTM sample the fibers were not oriented exactly perpendicular to the polished surface, which promotes top debonding as well [57]. However, in that case

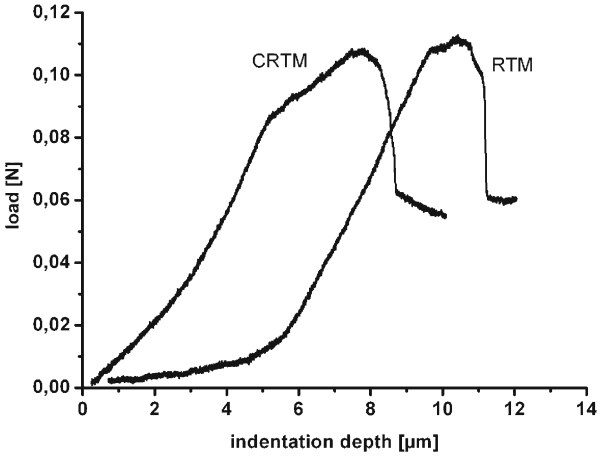

Fig. 6 Exemplary load-displacement curve RTM and CRTM

the effect on the measured maximum load is negligible [58]. Also in the present study no effects to the interfacial shear strength could be determined.

The interfacial shear strength of the TRTM samples were on average significantly lower than those of the thermoset RTM processes, which is due to a lower fiber-matrix adhesion. In addition to the material system, the interfacial shear strength may also be affected by the production, storage and preparation. While the effects of humidity are qualified with an appropriate coupling agent [13], the influence of grinding at the preparation and the subsequent storage is unknown. The porosity and the fiber content in the TRTM sample is also higher than in the RTM and CRTM samples, which can also weaken the interfacial properties by increased direct fiber-fiber contacts, as long as no chemical bonds between the fibers exists [4, 47, 59]. The large standard deviation of the interlaminar shear strengths can also conclude to large differences between the various interfaces. By factors such as the measured average porosity of 3.7 vol.-%, the loss of strength due to moisture absorption of the PA6 matrix and the direct fiber-fiber contacts, because of the increased fiber volume content, the fluctuations of the measured interfacial shear strength can be explained. However, it is not clear whether these are the only factors. Nonetheless, there appears to be no strengthened interfacial layer, neither by a coupling agent, nor by a nucleating agent induced interdiffusion. A macroscopic examination of the specimen confirmed the poor interfacial shear strengths, as during the preparation whole fiber bundles were pulled out.

Like for the thermosets before, only very few matrix particles at the visible interface of the pushed out fibers could be seen. It also seems to be a failure between fiber and interface layer. This could also not be directly confirmed, by coloring the matrix after the push out test. However, with an achieved maximum interfacial shear strength of 51.8 MPa and a measured matrix tensile strength of $R_{m,PA6}$ = 68 MPa it is obvious that the failure takes place at the interface B in Fig. 3. Compared with literature values of the same material system (glass fibers in PA 6) [13], a similar damage behavior and comparable interfacial shear strength values were shown.

The surface itself had many scratches and damage on the fiber edges (Fig. 7), which further amplifies the stress peak at the end of the fibers [60]. As a reason for the poor quality of the surface from the thermoplastic samples the difficult sample preparation can be mentioned.

Because of the low interlaminar shear strength and the high standard deviation the degree of crystallization of the thermoplastic polyamide 6 matrix was considered. For this purpose, a microtome cutted slice was observed under a polarization microscope. Crystalline regions can be seen as for example spherulites induced by interdiffusion. Figure 8 shows a direct comparison between an image of a TRTM sample with and without polarized light. Clearly visible are the black appearing amorphous fibers and the light shimmering crystalline structures in the matrix. It is striking that the matrix has a much lower crystallinity in the densely packed areas of fibers and that crystalline structures will only form sporadic inside the rovings.

Thus, the crystallization of the matrix increases, as soon as the fiber density decreases. The indentation of a fiber without the enhancing effect of spherulites requires less load [13], so that the high dispersion of the interface shear strength can be explained.

This formation of the crystalline regions also suggests that the visible spherulites do not have formed due to the topographical similarities with the coupling agent, but due to other effects. It is asserted that the used coupling agent of the fibers seems not to be compatible with the thermoplastic material system. The most obvious cause for the formation of spherulites is therefore the cooling rate of the matrix and the resulting induced nucleation. Below a temperature of 108 °C the nucleation rate of a polyamide 6 decreases dramatically to almost zero [61]. Because of the insertion temperature of the glass fibers of 80 °C into the mold and additionally the low thermal conductivity of E-glass, the formation of spherulites between the rovings will be significantly reduced.

The effect of the earlier discussed fiber breakage during the push out test could hardy be observed for the thermoplastic TRTM samples. Due to the low shear strength and thus low loading during the test, this result is quite obvious. However, the large scattering of the load maxima is also conspicuous.

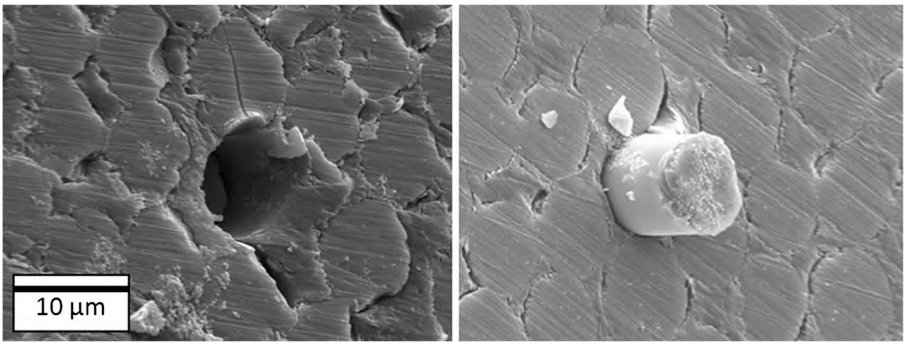

Fig. 7 SEM images of a TRTM specimen: push-out indentation (*left*) and a push-out extrusion (*right*)

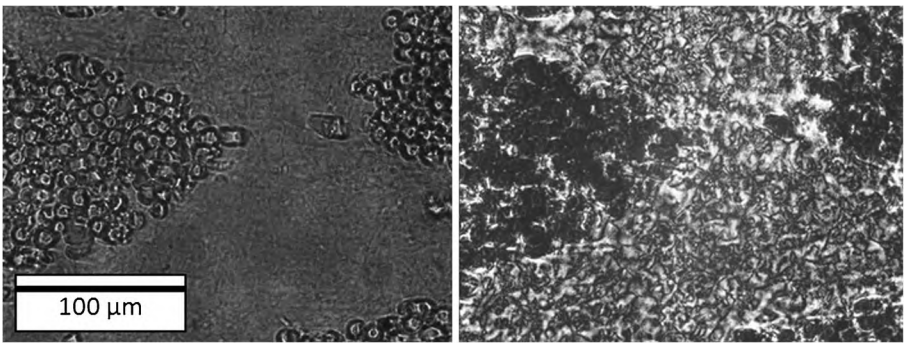

Fig. 8 Image of a microtome cut of a TRTM sample; without polarization (*left*); with polarization (*right*)

Summary and conclusion

The determined interfacial shear strength of RTM and CRTM were close together and with a value of approximately 80 MPa very high. This can be explained by a formation of an interfacial layer between the epoxy resin and the glass fibers. Differences were found in a higher damage rate of the indented fibers at the RTM process (> 80 %) compared to the CRTM process (15 %). As the reason for this behavior a top debonding of fibers in the CRTM process is suspected, through preparation induced interfacial damage on the upper end of the fiber. Also a specimen preparation which was not exactly perpendicular to the main fiber direction seems likely. Nevertheless both processes provide with the given combination of materials similar interfacial properties of high quality.

The push-out tests of TRTM process yielded significantly lower interfacial shear strength and a larger scatter compared with the thermosetting RTM processes. This could be attributed to the irregular crystallization of the matrix in regions of the fiber rovings. Further influencing factors on the interfacial shear strength as the porosity and the fiber content, as well as the the preparation by wet sanding also suggest lower shear strength. Due to the mechanical characteristics and the poor crystallization of the matrix at the interface can generally be assumed that the used coupling agent is not compatible to the thermoplastic matrix.

SEM images of the indented fibers suggested that no adherent matrix residues are present on the fibers in all material systems.

Acknowledgements The authors gratefully acknowledge Dr. Raman Chaudhari and Mr. Rainer Wendel for the manufacture of the RTM panels at the Fraunhofer ICT. They also appreciate the financial support from the KITe hy-LITE innovation cluster funded by the Fraunhofer Gesellschaft, the Karlsruhe Institute of Technology and the state of Baden-Württemberg.

References

1. Ehrenstein G (2006) Faserverbund-KKunststoffe. Carl Hanser Verlag, München
2. Godara A, Gorbatikh L, Kalinka G, Warrier A, Rochez O, Mezzo L, Luizi F, Vuure AV, Lomov S, Verpoest I (2010) Interfacial shear strength of a glass fiber/epoxy bonding in composites modified with carbon nanotubes. Compos Sci Technol 70:1346–1352

3. Janczak J, Rohr L, Schulz P, Degischer H (1995) Grenzflächenuntersuchungen an endlosfaserverstärkten Aluminiummatrix-Verbundwerkstoffen für die Raumfahrttechnik. Oberflächen - Werkstoff:14–20
4. Thomason JL (1995) The interface region in glass fibre-reinforced epoxy resin composites: 1. Sample preparation, void content and interfacial strength. Composites 26(7):467–475
5. Mittal K (1977) The role of the interface in adhesion phenomena. Polym Eng Sci 17(7):467–473
6. Sterman S, Marsden J (1966) Silane coupling agents. Reinforced Plastics Symposium 58(3):33–37
7. DiBenedetto A (2001) Tailoring of interfaces in glass fiber reinforced polymer composites: a review. Mater Sci Eng 30(2):74–82
8. Neitzel M, Mitschang P (2004) Handbuch verbundwerkstoffe - werkstoffe, verarbeitung, anwendung. Carl Hanser Verlag, München
9. Plueddemann E (1970) Adhesion through silane coupling agents. J Adhes 2(3):184–201
10. Sterman S, Marsden J (1966) The effect of silane coupling agents in improving the properties of filled or reinforced thermoplastics. Polym Eng Sci 6(2):97–112
11. Downing T, Kumar R, Cross W, Kjerengtroen L, Kellar J (2000) Determining the interphase thickness and properties in polymer matrix composites using phase imaging atomic force microscopy and nanoindentation. J Adhes Sci Technol 14(14):1801–1812
12. Griswold C, Cross W, Kjerengtroen L, Kellar J (2005) Interphase variation in silane-treated glass-fiber-reinforced epoxy composites. J Adhes Sci Technol 19(3–5):279–290
13. Bian X, Ambrosio L, Kenny J, Nicolais L, DiBenedetto A (1991) Effect of water absorption on the behaviour of E-glass fiber/nylon-6 composites. Polym Compos 12(5):333–337
14. Qian L, Bruce F, Kellar J, Winter R (1995) An instrument for testing interfacial shear strength in polymer matrix composites. Meas Sci Technol 6:1009–1015
15. Mäder E, Zhandarov S, Gao S, Zhou X-F, Nutt S (2002) Bond strength measurement between glass fibres and epoxy resin at elevated temperatures using the pull-out and push-out techniques. J Adhes 78:547–569
16. Chen E, Hsiao B (1992) Effects of transcrystalline interphase in advanced polymer composites. Polym Eng Sci 32(4):280–286
17. Campbell D, Qayyum M (1980) Melt crystallization of polypropylene: effect of contact with fiber substrates. Journal of Polymer Science: Polymer Physics Edition 18:83–93
18. Miller B, Muri P, Rebenfeld L (1987) A microbond method for determination of the shear strength of a fibre/resin interface. Compos Sci Technol 28:17–32
19. Kalinka G, Leistner A, Hampe A (1997) Characterisation of the fibre/matrix interface in reinforced polymers by the push-in technique. Compos Sci Technol 51:845–851
20. Feih S, Wonsyld K, Minzari D, Westmann P, Lilholt H (2004) Testing procedure for the single fiber fragmentation test. Risø National Laboratory, Roskilde, Dänemark
21. Kim J-K, Lu S, Mai Y-W (1994) Interfacial debonding and fibre pull-out stresses. J Mater Sci 29:554–561
22. G. Kalinka B. Neumann, Bestimmung von Interface-Festigkeit oder -Trennarbeit mit dem Pull-Out-Versuch. Bundesamt für Materialforschung und -prüfung (BAM), Berlin, 2005.
23. Qiu Y, Schwartz P (1991) A new method for study of the fiber-matrix interface in composites: single fiber pull-out from a microcomposite. J Adhes Sci Technol 5(9):741–756
24. Marshall DB (1984) An indentation method for measuring matrix-fiber frictional stresses in ceramic composites. J Am Ceram Soc 67(12):C259–C260
25. Bright J, Shetty D, Griffin C, Limaye S (1989) Interfacial bonding and friction in silicon carbide (filament)-reinforced ceramic- and glass-matrix composites. J Am Ceram Soc 72(10):1891–1898
26. Zhou X-F, Wagner H, Nutt S (2001) Interfacial properties of polymer composites measured by push-out and fragmentation tests. Compos Part A 32:1543–1551
27. Cox H (1952) The elasticity and strength of paper and other fibrous materials. Br J Appl Phys 3:72–79
28. Kelly A, Zweben C (1976) Poisson contraction in aligned fibre composites showing pull-out. J Mater Sci 11(3):582–586
29. Shetty D (1988) Shear-lag analysis of fiber push-out (indentation) tests for estimating interfacial friction stress in ceramic-matrix composites. J Am Ceram Soc 71(2):107–109
30. McCartney L (1989) New theoretical model of stress transfer between fibre and matrix in a uniaxially fibre-reinforced composite. Proceedings of the Royal Society A 425:215–144
31. Sigl LS, Evans AG (1989) Effects of residual stress and frictional sliding on cracking and pull-out in brittle matrix composites. Mech Mater 8(1):1–12
32. Kerans R, Parthasarathy T (1991) Theoretical analysis of the fiber pullout and pushout tests. J Am Ceram Soc 74(7):1585–1596
33. Hsueh CH, Rebillat F, Lamon J, Lara-Curzio E (1995) Analyses of fiber push-out tests performed on nicalon/SiC composites with tailored interfaces. Compos Eng 5(10–11):1387–1401

34. Nairn J (1997) On the use of shear-lag methods for analysis of stress transfer in unidirectional composites. Mech Mater 26:63–80
35. Bechel V, Sottos N (1998) Application of debond length measurements to examine the mechanics of fiber pushout. Journal of the Mechanics and Physics of Solids 46(9):1675–1697
36. Trimula S, Madanaraj H, Kaw A, Besterfield G, Ye J (1996) Effect of extrinsic and intrinsic factors on an indentation test. Int J Solids Struct 33(24):3497–3516
37. Wagner HD, Gallis HE, Wiesel E (1993) Study of the interface in Kevlar 49-epoxy composites by means of microbond and fragmentation tests: effects of materials and testing variables. J Mater Sci 28:2238–2244
38. Pisanova EV, Zhandarov SF, Dovgyalo VA (1993) Adhesive strength in thermoplastic polymer-thin fiber systems. Measured value as a function of the testing method. Mech Compos Mater 29(2):175–180
39. Pitkethly M, Favre J, Gaur U, Jakubowski J, Mudrich S, Caldwell D, Drzal L, Nardin M, Wagner H, Landro LD, Hampe A, Armistead J, Desaeger M, Verpoest I (1993) A round-robin programme on interfacial test methods. Compos Sci Technol 48(1–4):205–214
40. Zhandarov SF, Pisanova EV (1997) The local bond strength and its determination by fragmentation and pull-out tests. Compos Sci Technol 57(8):957–964
41. Potter K (1997) Resin transfer moulding. Springer
42. Young W-B, Chiu C-W (1995) Study on compression transfer molding. Composite Materials 29:2180–2191
43. Bickerton S, Abdullah M (2003) Modeling and evaluation of the filling stage of injection/compression moulding. Compos Sci Technol 63:1359–1375
44. Bitterlich M, Ehleben M, Wollny A, Desbois P, Renkl J, Schmidhuber S (2014) Thermoplastisches resin transfer moulding (T-RTM): maßgeschneidert auf reaktives polyamid 6. Kunststoffe 104(3):80–84
45. Lee L, Ottino J, Ranz W, Macosko C (1980) Impingement mixing in reaction injection molding. Polym Eng Sci 20(13):868–874
46. K. V. Rijswijk, H. Bersee, W. Jager S. Picken, Optimisation of anionic polyamide-6 for vacuum infusion of thermoplastic composites: choice of activator and initiator. *Compos Part A*, Bd. 37, pp. 949–956, 2006.
47. Merzkirch M, Weidenmann K, Kerscher E, Löhe D, Pietzka D, Schikorra M, Tekkaya A (2008) Mechanical Properties of Hybrid Composite Extrusions of an Aluminium-Alumina Wire Reinforced Aluminium Alloy. Material Science and Technology:2552–2562
48. Kallas M, Koss D, Hahn H, Hellmann J (1992) Interfacial stress state present in a “thin-slice” fibre push-out test. J Mater Sci 27:3821–3826
49. Huang C, Zhu D, Cong X-D, Kriven W (1997) Carbon-coated-glass-fiber-reinforced cement composites: I, fiber pushout and interfacial properties. J Am Ceram Soc 80(9):2326–2332
50. Moser B, Rossoll A, Weber L, Beffort O, Mortensen A (2003) Transmitted light microscopy of a fibre reinforced metal. J Microsc 209:8–12
51. Bechel V, Sottos N (1998) A comparison of calculated and measured debond lengths from fiber push-out tests. Compos Sci Technol 58:1727–1739
52. Chai Y, Mai Y-W (2001) New analysis on the fiber push-out problem with interface roughness and thermal residual stresses. J Mater Sci 36:2095–2104
53. Wu H, Dwight D, Huff N (1997) Effects of silane coupling agents on the interphase and performance of glass-fiber-reinforced polymer composites. Compos Sci Technol 57:975–983
54. Ehrenstein G (2011) Polymer werkstoffe. Carl Hanser Verlag, München
55. Cross W, Johnson F, Mathison J, Griswold C, Kellar J (2002) The effect of interphase curing on interphase properties and formation. J Adhes 78:571–590
56. Cook R, Pharr G (1990) Direct observation and analysis of indentation cracking in glasses and ceramics. J Am Ceram Soc 73(4):787–817
57. Brylka B, Fritzen F, Böhlke T, Weidenmann KA (2011) Influence of micro-structure on fibre push-out tests. Proc Appl Math Mech 11(1):141–142
58. Brylka B, Fritzen F, Böhlke T, Weidenmann K (2010) Study of experimental methods for interface problems based on virtual testing. Proc Appl Math Mech 10:109–110
59. Kelly A, Davies G (1965) The Principles of the Fibre Reinforcement of Metals. Metallurgical Reviews 10(37):17
60. Marotzke C (1994) The elastic stress field arising in the single-fiber pull-out test. Compos Sci Technol 50: 393–405
61. Krevelen DV (1997) Properties of polymers. Elsevier, Amsterdam